Inorg. Chem. **2005**, *44*, 1774–1785

Synthesis, Structural Characterization, and Molecular Modeling of Dodecaniobate Keggin Chain Materials

François Bonhomme,[†] James P. Larentzos,[‡] Todd M. Alam, Edward J. Maginn,[‡] and May Nyman*,[†]

Geochemistry Department, Sandia National Laboratories, Albuquerque, New Mexico 87185-0750, and Department of Chemical and Biomolecular Engineering, University of Notre Dame, 182 Fitzpatrick Hall, Notre Dame, Indiana 46556-5637

Received August 23, 2004

Four new isostructural one-dimensional dodecaniobate Keggin materials, $Na_{12}[Ti_2O_2][TNb_{12}O_{40}]\cdot xH_2O$ and $Na_{10}[Nb_2O_2][TNb_{12}O_{40}]\cdot xH_2O$ with T = (Si or Ge), have been synthesized hydrothermally using a Lindqvist-ion salt, $Na_7[Nb_6O_{19}H]\cdot 15H_2O$, as the precursor. Their structure, consisting of chains of Keggin ions $[TNb_{12}O_{40}]^{16-}$ linked by $[Ti_2O_2]^{4+}$ or $[Nb_2O_2]^{6+}$ bridges, was solved ab initio from powder diffraction data. The location of the charge-balancing sodium atoms and the water molecules was further investigated by molecular simulations. These compounds were also characterized by IR and solid-state ^1H, ^{29}Si, and ^{23}Na MAS NMR spectroscopies. The structural relationships between these and related phases based on similar Keggin ion building units are discussed.

Introduction

The use of polyoxometalates (POMs) as discrete building blocks for the synthesis of extended inorganic or hybrid organic/inorganic solids has attracted considerable interest in recent years.[1−5] The most commonly observed geometries of POM anionic clusters are the Keggin (e.g., $[SiW_{12}O_{40}]^{4-}$) and Dawson−Wells (e.g., $[P_2Mo_{18}O_{62}]^{6-}$) heteropolyanions.[6,7] It has been amply demonstrated that both these plenary clusters and their lacunary derivatives can be linked into multidimensional compounds, using both transition metals and lanthanides. Monovacant Keggin clusters chelating lanthanide cations can thus be assembled into linear or zigzag chains or even planes, depending on the nature of the rare-earth cation.[8,9] Plenary POMs capped with La^{3+} can be assembled together by polydentate organic ligands (such as squarate or glutarate) coordinating the lanthanum ions.[10] Extended solids have also been produced by linking POMs with a variety of transition metals that bridge two or more clusters and are also coordinated by organic or anionic ligands.[11−14] Purely inorganic assemblies of plenary polyoxometalates are more scarce: the most commonly observed geometry is a chain of linked bicapped α-Keggin ions formed by edge-sharing of the octahedral caps.[15−18] The α-Keggin ions have also been observed to form chains through an oxo ligand that bridges two metals belonging to adjacent clusters.[19,20]

* Corresponding author. E-mail: mdnyman@sandia.gov.
[†] Sandia National Laboratories.
[‡] University of Notre Dame.

(1) Khan, M. I. *J. Solid State Chem.* **2000**, *152*, 105.
(2) Johnson, B. J. S.; Schroden, R. C.; Zhu, C. C.; Young, V. G.; Stein, A. *Inorg. Chem.* **2002**, *41*, 2213.
(3) Khan, M. I.; Yohannes, E.; Doedens, R. J. *Inorg. Chem.* **2003**, *42*, 3125.
(4) Lisnard, L.; Dolbecq, A.; Mialane, P.; Marrot, J.; Secheresse, F. *Inorg. Chim. Acta* **2004**, 845.
(5) Lu, Y.; Xu, Y.; Wang, E.; Li, Y.; Wang, L.; Hu, C.; Xu, L. *J. Solid State Chem.* **2004**, *177*, 2210.
(6) Jeannin, Y. P. *Chem. Rev.* **1998**, *98*, 51.
(7) Pope, M. T. *Heteropoly and Isopoly Oxometalates*; Springer-Verlag: New York, 1983.
(8) Mialane, P.; Lisnard, L.; Mallard, A.; Marrot, J.; Antic-Fidancev, E.; Aschehoug, P.; Vivien, D.; Secheresse, F. *Inorg. Chem.* **2003**, *42*, 2102.
(9) Sadakane, M.; Dickman, M. H.; Pope, M. T. *Angew. Chem., Int. Ed.* **2000**, *39*, 2914.
(10) Dolbecq, A.; Mialane, P.; Lisnard, L.; Marrot, J.; Secheresse, F. *Chem. Eur. J.* **2003**, *9*, 2914.
(11) Liu, C.; Zhang, D.; Xiong, M.; Zhu, D. *Chem. Commun.* **2002**, 1416.
(12) Duan, L.; Pan, C.; Xu, J.; Cui, X.; Xie, G.; Wang, T. *Eur. J. Inorg. Chem.* **2003**, 2578.
(13) Bu, W.; Ye, L.; Yang, G.; Gao, J.; Fan, Y.; Shao, M.; Xu, J. *Inorg. Chem. Commun.* **2001**, *4*, 1.
(14) Pan, C.; Xu, J.; Li, G.; Chu, D.; Wang, T. *Eur. J. Inorg. Chem.* **2003**, 1514.
(15) Muller, A.; Koop, M.; Schiffels, P.; Bogge, H. *Chem. Commun.* **1997**, *97*, 1715.
(16) Nyman, M.; Bonhomme, F.; Alam, T. M.; Rodriguez, M. A.; Cherry, B. R.; Krumhansl, J. L.; Nenoff, T. M.; Sattler, A. M. *Science* **2002**, *297*, 996.
(17) Luan, G.; Wang, E.; Han, Z.; Li, Y. *Inorg. Chem. Commun.* **2001**, *4*, 541.
(18) Shivaiah, V.; Hajeebu, S.; Das, S. K. *Inorg. Chem. Commun.* **2002**, *5*, 996.
(19) Galan-Mascaros, J. R.; GimenezSaiz, C.; Triki, S.; Gomez-Garcia, C. J.; Coronado, E.; Ouahab, L. *Angew. Chem., Int. Ed. Engl.* **1995**, *34*, 1460.

10.1021/ic048847+ CCC: $30.25
Published on Web 02/09/2005

We are currently investigating the synthesis and crystal chemistry of new polyoxoniobate materials, both as extended solids composed of linked clusters and as soluble hydrated salts of isolated polyanions.[16,21,22] These compounds proved more challenging to synthesize than their polyoxomolybdate, -tungstate, and -vanadate counterparts[7] because of the lack of soluble monomeric precursors (such as Na_2WO_4 or Na_2MoO_4), which dictates the use of more severe synthetic methods such as hydrothermal processing. Furthermore, they form within a relatively narrow range of pH. The first heteropolyniobates were thus reported recently in 2002.[16] Polyoxoniobate-based materials are stable in alkaline media, whereas most other POMs are stable only under acidic conditions. These Nb^{5+}-based materials have much larger negative charges per cluster than the Mo^{6+}/W^{6+}-based materials. These two properties make polyoxoniobates attractive as high-capacity ion exchangers or cation sorbents for applications involving very basic media (e.g., radionuclide separation from caustic nuclear wastes).

The first material composed of linked heteropolyniobate clusters that has been reported is the one-dimensional $K_{12}[Ti_2O_2][SiNb_{12}O_{40}]\cdot 16H_2O$ (**K−Nb$_{12}$**), which features α-Keggin $[SiNb_{12}O_{40}]^{16-}$ ions linked together by $Ti_2O_2^{4+}$ bridges.[16] The current publication focuses on the synthesis and characterization of a series of one-dimensional dodecaniobate Keggin chain materials with sodium as the charge-balancing cation that are related to but not isostructural with the previously reported potassium phase. Four members of this family have been obtained, with either Si or Ge as the central tetrahedral atom and either $[Ti_2O_2]^{4+}$ or $[Nb_2O_2]^{6+}$ as the bridging unit. These four new compounds could only be obtained as microcrystalline powders, and their structures were solved and refined from X-ray powder diffraction data. Although we determined with reasonable accuracy the structure and relative arrangement of the Keggin chains from X-ray powder data, the location and differentiation of the sodium atoms and water molecules residing between the Keggin chains was difficult to achieve because of the similarity of their scattering factors and the high mobility of those species. The precise locations of the Na^+ ions and H_2O molecules were determined using molecular dynamics simulations based on the interaction of these species with each other and with the Keggin ion chains. Thermogravimetry was used to help quantify the amount of water contained in these chain materials.

Experimental Section

(1) Synthesis. (a) $Na_{12}[Ti_2O_2][SiNb_{12}O_{40}]\cdot xH_2O$ (Nb−Si−Ti). (i) NaOH/Nb_2O_5 Route. Sodium hydroxide (1.30 g, 32.5 mmol) was dissolved in 40 mL of DI water in a 100-mL Teflon-lined steel autoclave. Amorphous hydrous niobium oxide ($Nb_2O_5\cdot xH_2O$; 1.75 g, 10 mmol of Nb; Reference Metals Co. Inc., Bridgeville, PA), tetraethyl orthosilicate (TEOS; 0.90 g, 4.4 mmol), and tetraisopropyltitanium (TIPT; 1.25 g, 4.4 mmol) were added to the NaOH aqueous solution, and the mixture was stirred for 30 min. The mixture was then hydrothermally treated at 190 °C for 16 h. The resulting fine white powder was collected by vacuum filtration, washed with warm water and then ethanol, and dried in air at room temperature. The yield was ∼95% based on Nb.

(ii) Hexaniobate Route. Sodium hexaniobate[23] ($Na_7H_3O[Nb_6O_{19}]\cdot 14H_2O$; 2.85 g, 13.2 mmol of Nb, prepared as described previously[24]), TEOS (0.23 g, 1.1 mmol), and TIPT (0.65 g, 2.3 mmol) were added to 40 mL of DI water in a 100-mL Teflon-lined steel autoclave. The mixture was stirred for 5 min and then hydrothermally treated at 190 °C for 16 h. The yield was ∼33% based on Nb.

(b) $Na_{12}[Ti_2O_2][GeNb_{12}O_{40}]\cdot xH_2O$ (Nb−Ge−Ti). Sodium hexaniobate (0.57 g, 2.6 mmol of Nb), tetraethoxygermane [$Ge(OC_2H_5)_4$, 0.22 g, 0.87 mmol; (Gelest, Inc., Morrisville, PA), and TIPT (0.13 g, 0.46 mmol) were added to 8 mL of DI water in a 23-mL Teflon-lined steel autoclave. The mixture was stirred for 30 min and then hydrothermally treated at 200 °C for 16 h. The yield was ∼15% based on Nb.

(c) $Na_{10}[Nb_2O_2][SiNb_{12}O_{40}]\cdot xH_2O$ (Nb−Si−Nb). Sodium hexaniobate (0.57 g, 2.6 mmol of Nb) and TEOS (0.27 g, 1.1 mmol) were added to 8 mL of DI water in a 23-mL Teflon-lined steel autoclave. The mixture was stirred for 2 min and then hydrothermally treated at 190 °C for 17 h. The yield was ∼10% based on Nb.

(d) $Na_{10}[Nb_2O_2][GeNb_{12}O_{40}]\cdot xH_2O$ (Nb−Ge−Nb). Sodium hexaniobate (0.57 g, 2.6 mmol of Nb) and tetraethoxygermane (0.33 g, 1.30 mmol) were added to 8 mL of DI water in a 23-mL Teflon-lined steel autoclave. The mixture was stirred for 30 min and then hydrothermally treated at 190 °C for 20 h. The yield was ∼15% based on Nb.

(2) Characterization. X-ray powder diffraction was performed with a Bruker D8 Advance diffractometer in Bragg−Brentano geometry with Ni-filtered Cu Kα radiation. The specimen was rotated at 0.5 Hz to improve particle statistics. The sample density was determined using a Micromeritics AccuPyc 1330 helium displacement pycnometer. Solid-state ^{29}Si MAS NMR spectra were obtained on a Bruker AMX400 console at a resonant frequency of 79.46 MHz, using a 7-mm broadband MAS probe spinning at 4 kHz at room temperature. Samples were spun with air to reduce the ^{29}Si spin lattice relaxation time. The spectra were obtained using a single-pulse Bloch decay, with inverse-gated high-power ^{1}H decoupling using 64 scan averages, a 5-μs $\pi/2$ pulse, and a 360-s recycle delay. Chemical shifts were referenced to the secondary standard Q_8M_8 ($\delta = +11.4$ ppm) with respect to TMS ($\delta = 0.0$ ppm). Solid-state ^{23}Na MAS NMR spectra were obtained on a Bruker AMX400 instrument at a resonant frequency of 105.81 MHz, using a 4-mm broadband probe spinning at 12.5 kHz. Typical experimental conditions were a 2-μs ($\pi/6$) pulse, a 2-s recycle delay, and 64 scan averages. Chemical shifts were referenced to the external standard 1 M NaCl ($\delta = 0.0$ ppm). Solid-state ^{1}H MAS NMR of the original **Nb−Si−Ti** and ^{2}H-exchanged material were obtained on a Bruker Avance 600 NMR instrument operating at 600.1 MHz. The ^{1}H spectra were obtained using a 4-mm MAS probe spinning at 10 kHz, with a 2-μs $\pi/2$ pulse, a 2-s recycle delay, and 16 scan averages. The extent of exchange was determined by normalizing the spectral integrals with respect to sample weight. Infrared spectra (370−4000 cm^{-1}) were recorded on a Perkin-Elmer

(20) Yan, B.; Xu, Y.; Bu, X.; Goh, N. K.; Chia, L. S.; Stucky, G. D. *J. Chem. Soc., Dalton Trans.* **2001**, 2009.
(21) Nyman, M.; Bonhomme, F.; Alam, T. M.; Parise, J. B.; Vaughan, G. M. B. *Angew. Chem., Int. Ed.* **2004**, *43*, 2787.
(22) Nyman, M.; Criscenti, L. J.; Bonhomme, F.; Rodriguez, M. A.; Cygan, R. T. *J. Solid State Chem.* **2003**, *176*, 111.
(23) Goiffon, A.; Philippot, E.; Maurin, M. *Rev. Chim. Miner.* **1980**, *17*, 466.
(24) Alam, T. M.; Nyman, M.; Cherry, B. R.; Segall, J. M.; Lybarger, L. E. *J. Am. Chem. Soc.* **2004**, *126*, 5610.

Table 1. Crystal Data and Structure Refinement Parameters for **Nb−Si−Ti**

compound	$Na_{12}[Ti_2O_2][Nb_{12}SiO_{40}]\cdot 4H_2O$
formula weight	2259 g/mol
crystal system	tetragonal
space group	$I\bar{4}m2$ (No. 119)
unit cell dimensions	$a = 14.2701(5)$ Å
	$c = 11.2923(7)$ Å
volume	2299.5(2) Å^3
Z	2
density (measured)	3.25(2) g/cm^3
density (calculated)	3.26 g/cm^3
temperature	298(2) K
wavelength	Cu $K_{\alpha 1,\alpha 2}$
2θ range	5.0−120.0°
step size 2θ	0.04°
time per step	25 s
min fwhm	0.08°
no. of independent atoms	16
no. of free parameters[a]	86
no. of structural parameters[a]	35
no. of "independent" reflections	521
final R indices	$R_p = 5.62\%$, $R_{wp} = 7.44\%$
	$R_{exp} = 3.37\%$, $\chi^2 = 4.88$
	$R_{Bragg} = 4.72\%$
soft constraints	$Nb-O_{terminal} = 1.78(1)$ Å
	$Nb-O_{bridging} = 1.99(1)$ Å
	$Nb-O_{central} = 2.42(1)$ Å
	$Ti-O_{cluster} = 2.02(1)$ Å
	$Ti-O_{bridging} = 1.89(1)$ Å
	$Si-O_{central} = 1.64(1)$ Å
	$Ti-Ti = 2.92(1)$ Å
	$O_{central}-Nb-O_{terminal} = 165(1)°$
	$O-Si-O = 109.5(10)°$

[a] 32 positional parameters and 3 isotropic atomic displacement parameters; 12 profile parameters and 39 linearly interpolated background points.

Spectrum GX FTIR spectrometer using the KBr pellet method. Samples were examined with a JEOL JSM-6300V scanning electron microscope equipped with a Link GEM Oxford detector and IRIDIUM IXRF Systems software for EDAX analysis. Thermal analysis was performed with a TA Instruments SDT 2960 simultaneous TGA-DTA apparatus under nitrogen flow with a heating rate of 10 °C/min. Elemental analysis was executed on a Perkin-Elmer Sciex Elan 6100 ICP-MS instrument using an argon plasma flame.

(3) Structure Determination. Because no suitable single crystal was obtained for any of the four phases reported, an *ab initio* structure determination from powder diffraction data was carried out for compound **Nb−Si−Ti**. The positions of the first 20 peaks were refined with the program XFIT[25] using a split Pearson VII function for the more asymmetric low-angle peaks and a pseudo-Voigt function for the peaks above 20°. The peak positions were calibrated using NIST Silicon SRM640 as external standard. The pattern was then indexed with high figures of merit[26] ($M_{20} = 47$, $F_{20} = 52$) by the program TREOR90[27] with a tetragonal cell of approximate cell parameters $a = 14.28$ Å and $c = 11.30$ Å with $V = 2304$ Å^3. The refined lattice constants are given Table 1. The reflection conditions are only those of a body-centered cell. A whole-pattern profile refinement by the Le Bail method[28] (program FULLPROF2K[29]) with the space group *I*4/*mmm* confirmed the adequacy of this cell and systematic absences. The structure was initially solved in *I*4/*mmm* with the intensities extracted by the Le Bail refinement and the program DIRDIF[30] using Patterson map interpretation. The positions of three independent heavy atoms were immediately revealed along with several sites that could be attributed to oxygen atoms. At that stage, the infinite chains of linked Keggin anions similar to those found in $K_{12}[Ti_2O_2][SiNb_{12}O_{40}]\cdot 16H_2O$ (**K−Nb$_{12}$**)[16] or $K_{6.5}Na_{0.5}[V_2O_2][VMo_8V_4O_{40}]\cdot 12.5H_2O$ (**MoV**)[15] were recognized, which allowed for a rapid completion of the structure by manual build-up. **MoV** is also tetragonal, with a lattice constant *a* close to that of **Nb−Si−Ti** but with a double *c* axis. No extra peak whose indexation would require doubling of the *c* axis was detected in the diffraction pattern of **Nb−Si−Ti**. The coordinates of the oxygen atoms belonging to the chain of clusters were refined using bond distance and angle constraints (see Table 1) corresponding to the average values observed in the related phase **K−Nb$_{12}$**. The positions of the sodium atoms and/or water molecules, hardly distinguishable, were found by successive Rietveld refinement and difference Fourier map analysis. These sites were given the scattering factor of Ne, intermediate between those of Na and H_2O. The application of the bond valence sum method[31,32] to distinguish between these sites is difficult because of the large imprecision of the bond distances derived from Rietveld refinement and the likelihood of partial or mixed occupancy. The description in *I*4/*mmm* leads to a disordered distribution for the oxygen atoms (having 50% occupancy) around the silicon in the center of the Keggin clusters as well as for the oxygen atoms bridging the clusters together in an infinite chain. We therefore opted to lower the symmetry to the subgroup $I\bar{4}m2$, which allows for an ordered model of the central SiO_4 tetrahedron and gives more flexibility in modeling the sodium and water sites. Similarly to what is observed for **K−Nb$_{12}$**, no mixed occupancy on the Nb and Ti sites was evidenced; the population parameters of the transition metals refined to full occupancy, thus validating the assignment of the species. Further, the Nb/Ti ratio determined by ICP-MS was 5.8:1, in good agreement with the ratio of 6:1 expected from the structure determination. The refinement of the population parameter of the sodium or water sites showed that the two sites located on a general position were half-occupied. The number of water molecules per formula unit was determined by subtracting the number of sodium atoms necessary for charge balance from the number of occupied sites. The final difference Fourier map did not reveal any residual electron density that could be attributed to extra water molecules. The refinement eventually converged to a satisfactory agreement factor, $R_{Bragg} = 4.72\%$. The summary of crystallographic data, including the values of the geometrical constraints and measurement conditions, is given in Table 1. Atomic coordinates are presented in Table 2, and selected interatomic distances are given in Table 3. The observed, calculated, and difference Rietveld plots are shown in Figure 1.

The structure of the Nb-bridged counterpart **Nb−Si−Nb** was refined starting with a similar structural model for the Keggin ion chains, replacing the Ti site by Nb and using a similar set of bond and angle constraints. The locations of the various Na and/or water sites were found by difference Fourier maps analyses. The final agreement factor is $R_{Bragg} = 8.31\%$. The refined atomic coordinates are available as Supporting Information. No structural refinement was carried out for the two isoelectronic Ge-based phases **Nb−**

(25) Cheary R. W.; Coelho A. A. *J. Appl. Crystallogr.* **1992**, *25*, 109.
(26) de Wolff, P. M. *J. Appl. Crystallogr.* **1972**, *5*, 243.
(27) Werner, P. E.; Eriksson, L.; Westdahl, M. *J. Appl. Crystallogr.* **1985**, *18*, 367.
(28) Le Bail, A.; Duroy, H.; Fourquet, J. *Mater. Res. Bull.* **1988**, *23*, 447.
(29) Rodriguez-Carvajal, J. A. In *Collected Abstracts of Powder Diffraction Meeting*; Toulouse, France, 1990; p 127.
(30) DIRDIF96 program system. Beurskens, P. T.; Beurskens, G.; Bosman, W. P.; de Gelder, R.; Garcia-Granda, S.; Gould, R. O.; Israel, R.; Smits, J. M. M. Crystallography Laboratory, University of Nijmegen, Nijmegen, The Netherlands, 1996.
(31) Brese, N. E.; O'Keeffe, M. *Acta Crystallogr.* **1991**, *B47*, 192.
(32) Brown, I. D.; Altermatt, D. *Acta Crystallogr.* **1985**, *B41*, 244.

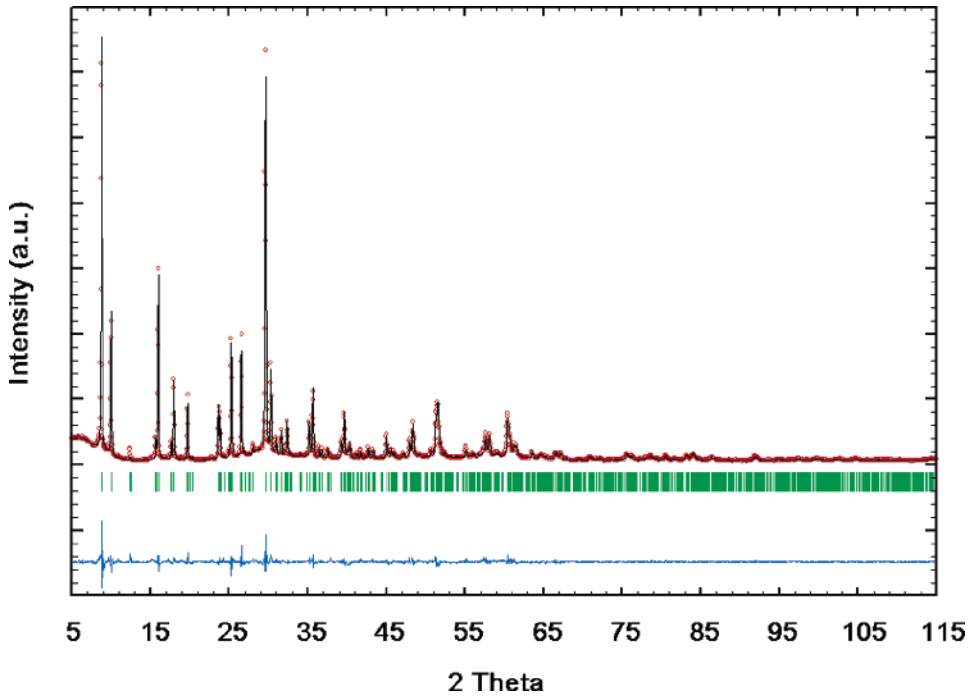

Figure 1. Observed, calculated, and difference Rietveld plots for **Nb**−**Si**−**Ti**.

Table 2. Atomic Coordinates from Rietveld Refinement for **Nb**−**Si**−**Ti**[a]

atom	site	*x*	*y*	*z*	population (%)
Nb1	16*j*	0.8704(3)	0.1335(3)	0.2163(2)	
Nb2	8*i*	0	0.2568(2)	0.9976(6)	
Ti	4*e*	0	0	0.3701(4)	
Si	2*a*	0	0	0	
O1	8*i*	0	0.3836(6)	0.005(6)	
O2	16*j*	0.837(1)	0.202(1)	0.339(1)	
O3	8*i*	0	0.118(1)	0.274(2)	
O4	8*i*	0	0.886(1)	0.735(2)	
O5	16*j*	0.7572(9)	0.090(1)	0.135(1)	
O6	16*j*	0.236(1)	0.892(1)	0.896(2)	
O7	8*i*	0.0970(5)	0	0.0833(9)	
O8	8*i*	0.081(1)	0	0.5000(−)	50
site 1	8*g*	0.747(1)	0.253(−)	0	100
site 2	8*h*	0.394(1)	0.106(−)	1/4	100
site 3	16*j*	0.267(2)	0.041(2)	0.458(3)	50
site 4	16*j*	0.099(2)	0.458(2)	0.164(3)	50

[a] Isotropic atomic displacement parameters: B(Nb) = B(Ti) = B(Si) = 2.9(1) Å^2, B(O) = 3.0(2) Å^2, B(Na/H_2O) = 6.0(4) Å^2.

Table 3. Selected Bond Lengths (Å) for **Nb**−**Si**−**Ti**

Nb1−O2	1.77(2)	Nb2−O1	1.81(1)
Nb1−O3	1.97(1)	Nb2−O5	1.98(2) 2x
Nb1−O4	1.99(2)	Nb2−O6	1.97(2) 2x
Nb1−O5	1.96(1)	Nb2−O7	2.45(1)
Nb1−O6	1.96(2)	Ti−O3	2.00(2) 2x
Nb1−O7	2.47(1)	Ti−O4	2.01(2) 2x
Si−O7	1.67(1) 4x	Ti−O8	1.86(1) 2x

Ge−**Ti** and **Nb**−**Ge**−**Nb**; the comparison of their diffraction pattern confirms that they are isostructural with their Si-based counterparts.

(4) Molecular Modeling. Given the difficulty in determining the actual positions of Na^+ and H_2O in the Keggin chain materials, molecular modeling studies were carried out on **Nb**−**Si**−**Ti** and **Nb**−**Si**−**Nb**. A complete description of the modeling procedure and force field is provided elsewhere;[33] only the essential modeling details specific to the present work are reported here. Although there have been studies that model lattice relaxation effects, we could not locate a suitable set of parameters that enabled accurate determination of the lattice parameters for these phases. We have found that the force-field potential that we have used in previous work accurately predicts cation and water positions but is incapable of accurately predicting the cell constants for these materials; thus we constrained the framework atoms of structures **Nb**−**Si**−**Ti** and **Nb**−**Si**−**Nb** to the experimentally determined positions while permitting Na^+ and H_2O to move. It was initially assumed that there were four water molecules present per Keggin cluster in the $Na_{12}[Ti_2O_2][SiNb_{12}O_{40}]\cdot 4H_2O$ (**Nb**−**Si**−**Ti**) material and six water molecules per Keggin cluster in the $Na_{10}[Nb_2O_2][SiNb_{12}O_{40}]\cdot 6H_2O$ (**Nb**−**Si**−**Nb**) structure as determined from the Rietveld refinements. The number of sodium atoms per formula unit was constrained by charge-balancing considerations. Both structures contain a 50% occupied oxygen O8 bridging atom site. This disorder is modeled by filling one-half of the O8 sites with oxygen atoms and assuming that the locally populated bridging sites will be the greatest possible distance apart from each other. A 2 × 2 × 2 supercell was used in the simulations, with all symmetry constraints removed for the sodium and water sites.

A simulated annealing molecular dynamics (MD) protocol was used, in which high-temperature simulations (ca. 1500 K) were initiated, followed by an annealing schedule in which the temperature was gradually lowered to 300 K. This procedure ensures that, at high temperature, the cations and water molecules are able to probe a sufficient number of configurations on the time scale of the simulations. As the temperature is lowered, the mobile species localize in their equilibrium positions, which are then recorded as the preferred positions. All simulations were performed using the General Utility Lattice Program (GULP).[34] Full periodic boundary conditions were employed with an interaction cutoff of 11.2 Å. The leapfrog finite-difference algorithm was used to determine the positions of the moveable atoms at each MD time step. The simulations were carried out for at least 500 ps, using a 1-fs time

(33) Larentzos, J. P.; Clearfield, A.; Tripathi, A.; Maginn, E. J. *J. Phys. Chem. B* **2004**, *108*, 17560.

(34) Gale, J. D. *J. Chem. Soc., Faraday Trans.* **1997**, *93*, 629.

Table 4. Simulated Atomic Coordinates and Population Fractions of Sodium Cations and Water Molecules Present in the **Nb−Si−Ti** Structure

site	*x*	*y*	*z*	standard deviation (Å)	deviation from experiment (Å)	population fraction
site 1 − Na^+/H_2O	0.743	0.257	0	0.36	0.08	100.0/0.0
site 2 − Na^+/H_2O	0.356	0.144	1/4	0.49	0.77	98.1/1.0
site 3 − Na^+/H_2O	0.234	0.069	0.504	0.83	0.80	26.8/11.8
site 4 − Na^+/H_2O	0.041	1/2	0.128	0.76	1.02	7.8/5.4

Table 5. Simulated Atomic Coordinates and Population Fractions of Sodium Cations and Water Molecules Present in the **Nb−Si−Nb** Structure

site	*x*	*y*	*z*	standard deviation (Å)	deviation from experiment (Å)	population fraction
site 1 − Na^+/H_2O	0.740	0.260	0	0.30	0.12	100.0/0.0
site 2 − Na^+/H_2O	0.361	0.139	1/4	0.52	0.76	93.3/3.9
site 3 − Na^+/H_2O	0.257	0	0.502	0.99	0.41	4.2/22.7
site 4 − Na^+/H_2O	0.040	1/2	0.119	0.71	0.82	19.5/8.8

Table 6. Simulated Atomic Coordinates and Population Fractions of Sodium Cations and Water Molecules Present in a **Nb−Si−Ti·14.5H_2O** Structure

site	*x*	*y*	*z*	standard deviation (Å)	deviation from experiment (Å)	population fraction
site 1 − Na^+/H_2O	0.750	0.250	0	0.39	0.06	98%
site 2 − Na^+/H_2O	0.377	0.123	1/4	0.97	0.34	74%
site 3 − Na^+/H_2O	0.274	0.071	0.488	0.91	0.55	17%
site 4 − Na^+/H_2O	0.110	0.440	0.176	1.03	0.33	16%

step. The long-range forces were evaluated with the Ewald summation method.[35]

Configurations from the MD trajectories containing the instantaneous positions of all Na^+ ions and H_2O molecules were saved at 0.25-ps intervals. Analysis of these configurations yields the relative probability of a Na^+ or H_2O locating in a particular position. To obtain the averaged atomic coordinates from the simulations, the positions of Na^+ and H_2O in each snapshot were classified by the nearest experimental site (within a 2.0 Å cutoff), folded by the $I\bar{4}m2$ symmetry operations and finally averaged over all snapshots in the entire simulation. The standard deviation is then computed by measuring the fluctuations about the averaged position. The magnitude of this fluctuation gives an indication of the relative mobility of Na^+ and H_2O. In general, approximately 90% of the Na^+ cations but only 30% of the H_2O molecules could be related to an experimental site within a 2.0-Å cutoff. The remaining Na^+ and H_2O could not be attributed to an experimental site and are treated as being located between sites. Finally, a "population fraction" was computed by monitoring the fraction of time a site was occupied by a given species over the entire simulation. This essentially gives the fraction of time that a particular experimental site is associated with Na^+ or H_2O during the simulation and is a relative measurement of the attractiveness of the site. The atomic positions reported in Tables 4−6 are idealized by the space-group symmetry, i.e., the raw averaged coordinates (usually that of a general position 16*j*) were shifted, if applicable, onto a nearby site with higher point symmetry. For example, site 1 in Table 5 was shifted from its original general position (16*j*: 0.741, 0.262, 0.000) to (8*g*: 0.740, 1 − *x*, 0). The shifts for the well-defined sites 1 and 2 were in any case smaller than 0.05 Å and were always less than 20% of their associated standard deviations for the more diffuse sites 3 and 4.

Results and Discussion

(1) Synthesis. Nb−Si−Ti was initially synthesized hydrothermally using amorphous hydrated niobium oxide and silicon and titanium alkoxides in a sodium hydroxide solution. An excess of both Ti and Si had to be used to prevent the formation of competing phases, such as $Na_{16}[SiNb_{12}O_{40}]\cdot 4H_2O$ [21] or $Na_8[Nb_8Ti_2O_{28}]\cdot 34H_2O$.[22] Similarly, varying the concentration of NaOH gave multiphase samples, unsuitable for structure determination. Although the samples obtained by this $NaOH/Nb_2O_5$ method were X-ray pure, they nevertheless contained sizable amount of amorphous impurities, likely hydrous sodium titanates as observed by SEM/EDAX. Longer reaction times lead to thermodynamically more stable compounds such as niobium based perovskites. However, we found that after 1 h of reaction at 190 °C, sodium hexaniobate[23] is the only crystalline phase that precipitates. Using this intermediate phase as a soluble Na and Nb precursor, without adding NaOH to the solution, allowed us to obtain products of higher purity, with a markedly improved crystallinity. The Nb-bridged phases could be obtained, albeit with a low yield, only by this synthetic route. The pH of the reactions using the hexaniobate ranges from 10.0 to 11.2 versus about 12.5 for the $NaOH/Nb_2O_5$ route. This decrease in basicity likely helps to stabilize the Nb-bridged phases that appear to be less stable than their Ti-bridged counterparts. By the $NaOH/Nb_2O_5$ route, we could not lower the pH below ∼12 and still obtain the desired phases as well-crystallized products.

(2) Description of the Keggin Chains. The structure of **Nb−Si−Ti** is composed of infinite chains formed of $[SiNb_{12}O_{40}]^{16-}$ clusters alternating with bridging $[Ti_2O_2]^{4+}$ units. These chains, running parallel to the *c* axis, carry a charge of −12 per cluster, which is balanced by 12 sodium ions. The $[SiNb_{12}O_{40}]^{16-}$ clusters exhibit the classical α-Keggin geometry,[6] with a central SiO_4 tetrahedron surrounded by four triads of edge-sharing distorted NbO_6 octahedra. Each titanium atom of the dimeric bridge is octahedrally coordinated. It is bound to four of the Keggin oxygen atoms (O3 and O4) that frame a 4-ring "window", and two additional oxygen atoms (O8) are shared with the titanium capping the adjacent cluster on the chain. Therefore, each TiO_6 octahe-

(35) Allen, M. F.; Tildesley, D. J. *Computer Simulation of Liquids*; Oxford Science Publications: Oxford, U.K., 1987.

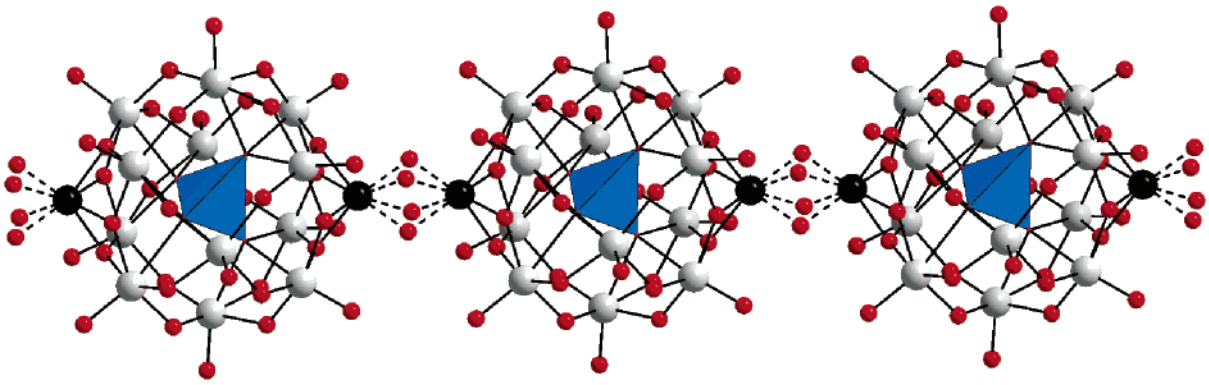

Figure 2. Infinite chains formed by $[SiNb_{12}O_{40}]^{16-}$ and $[Ti_2O_2]^{4+}$ dimers in **Nb−Si−Ti**.

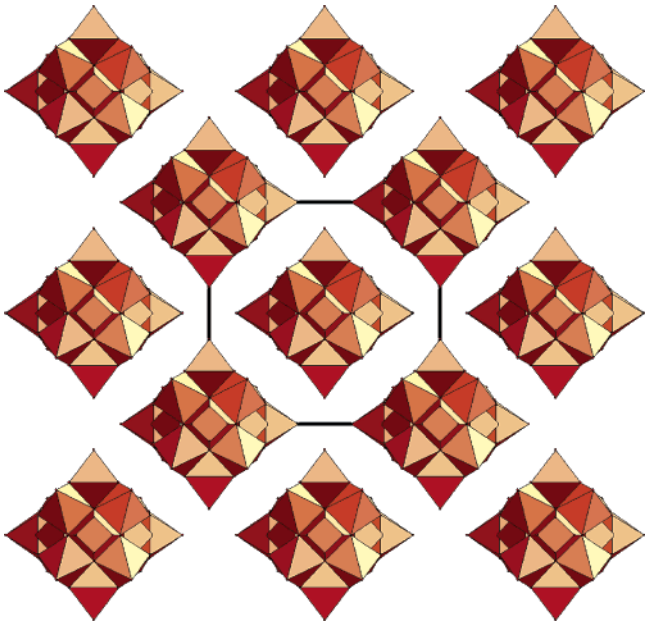

Figure 3. Polyhedral representation of the chains in **Nb−Si−Ti**, viewed along the *c* axis. (Cations and water molecules omitted.)

dron share edges with four NbO_6 octahedra within one Keggin cluster and with one other TiO_6 octahedron. This constrained geometry gives rise to strong angular distortions with O−Ti−O bond angles ranging from 72° to 117°. The O8 site, which is bonded to two titanium atoms, is disordered with a 50% occupancy factor (see Figure 2). The same type of disorder in the bridging species is observed in a related heteropoly tungstovanadate.[18] The type of infinite chains present in **Nb−Si−Ti** is also encountered in two other related tetragonal phases, $K_{12}[Ti_2O_2][SiNb_{12}O_{40}]\cdot 16H_2O$ (**K−Nb$_{12}$**)[16] and $K_{6.5}Na_{0.5}[V_2O_2][VMo_8V_4O_{40}]\cdot 12.5H_2O$ (**MoV**).[15] The main difference between these structures thus lies in the way the chains are packed together. The projections along the *c* axis of the structure of **Nb−Si−Ti** and **MoV** are identical, each chain being surrounded by four others in a checkered pattern (see Figure 3) and with the faces of adjacent chains facing each other. The disposition of the chains along the *c* direction is, however, different in these two phases. In **MoV**, the clusters belonging to neighboring chains lie in the same plane at constant *z* (see Figure 4a). This creates large void spaces around the bridging units where nonframework atoms can reside. On the contrary, adjacent chains in **Nb−Si−Ti** are shifted with respect to each other by one-half Keggin subunit along the *c* axis, so that the centers of the clusters of one chain are located in the planes containing the bridging moieties of the four surrounding chains (see Figure 4b). This staggered packing leads to a more compact structure, the free volume available to the cations and the water molecules (calculated with the program CERIUS2[36]) being 515 Å^3 per Keggin for **Nb−Si−Ti**, 16% smaller than the calculated void volume in **MoV** (600 Å^3 per Keggin). In **K−Nb$_{12}$**, the chains are rotated so that the corners of the squares, defined by the direction of the equatorial Nb−O$_t$ bond of the Keggin clusters, are facing each others in projection (see Figure 5). This mode of packing creates approximately cylindrical tunnels running along the *c* axis, with an accessible diameter of about 8 Å (see Figure 5). More than 70% of the total number of water molecules and charge-balancing potassium atoms reside in these channels. With a free volume of 790 Å^3 per Keggin, the structure of **K−Nb$_{12}$** is far more open than that of **Nb−Si−Ti** and **MoV**. Although **Nb−Si−Ti** and **K−Nb$_{12}$** contain the same type of infinite Keggin chains, their structures are very different and one phase cannot be converted into the other by ion exchange. Furthermore, by varying the synthesis conditions, we have never observed the formation of either the sodium analogue of **K−Nb$_{12}$** nor the potassium analogue of **Nb−Si−Ti**.

The cell parameters of the four title compounds, refined by the Le Bail method using NIST Si SRM640 as an internal standard, are reported in Table 7. The cell parameter along the Keggin chains (*c* axis) varies more than the *a* parameter, along which the chains are separated by sodium and water: $\Delta c/c = 0.90\%$ versus $\Delta a/a = 0.15\%$. As expected, the *c* axis increases with the size of both the tetrahedral and the bridging atoms. Although the ionic radius of Ge^{4+} is much larger than that of Si^{4+} ($R_{Ge} = 0.67$ Å, $R_{Si} = 0.54$ Å),[37] the difference in the *c* axis of the corresponding phases is only on the order of 0.03 Å, showing that the size of the Keggin ion is mostly independent of the radius of the central atom. A larger central TO_4 tetrahedron can therefore easily be accommodated by a slight shortening of the Nb−O$_{central}$ bond distances or by a decrease of the O$_{terminal}$−Nb−O$_{central}$ bond angle without increasing the diametric Nb−Nb distances. On

(36) *Cerius2−4.0 User Guide*, 4.2 ed.; Accelerys, Inc.: San Diego, CA, 1999.
(37) Shannon, R. D. *Acta Crystallogr.* **1976**, *A32*, 751.

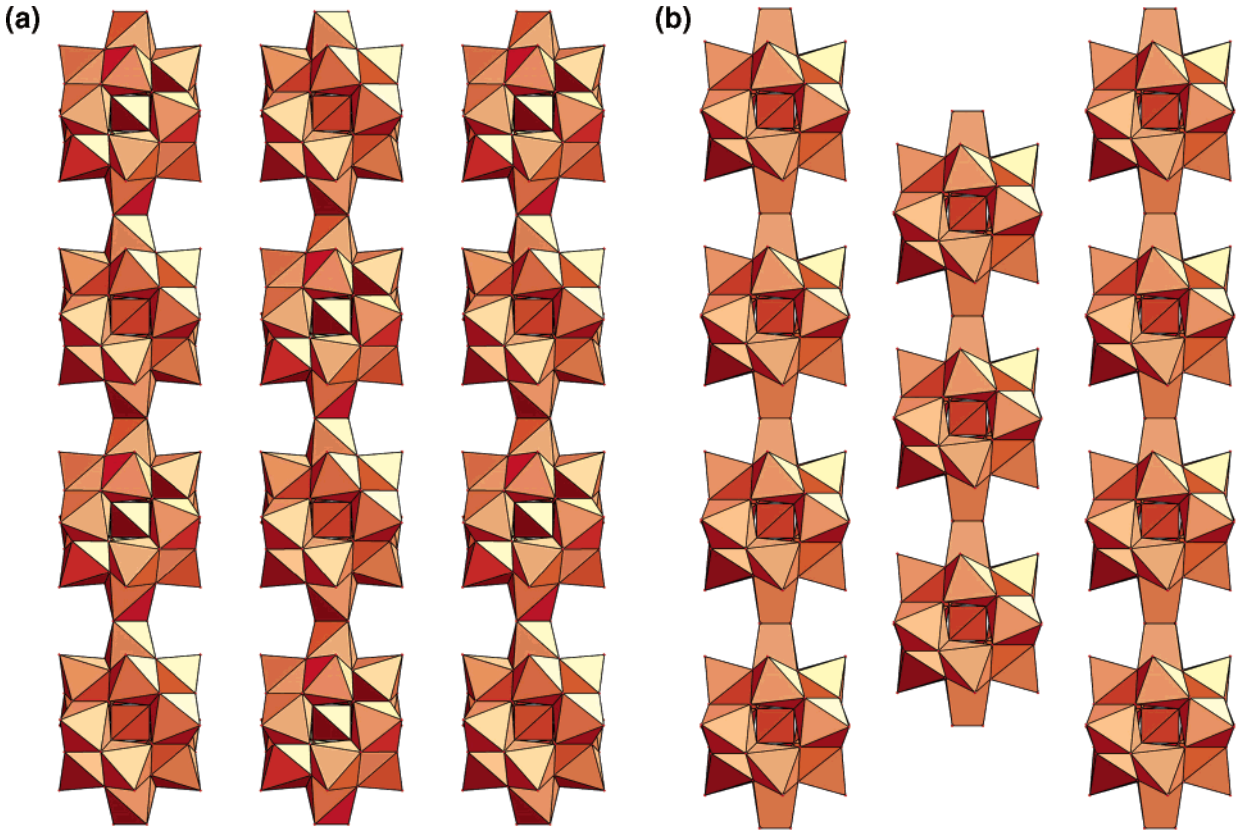

Figure 4. Polyhedral representation of the chains in (a) **MoV** and (b) **Nb−Si−Ti**, viewed along the *ab* plane. (Cations and water molecules omitted.)

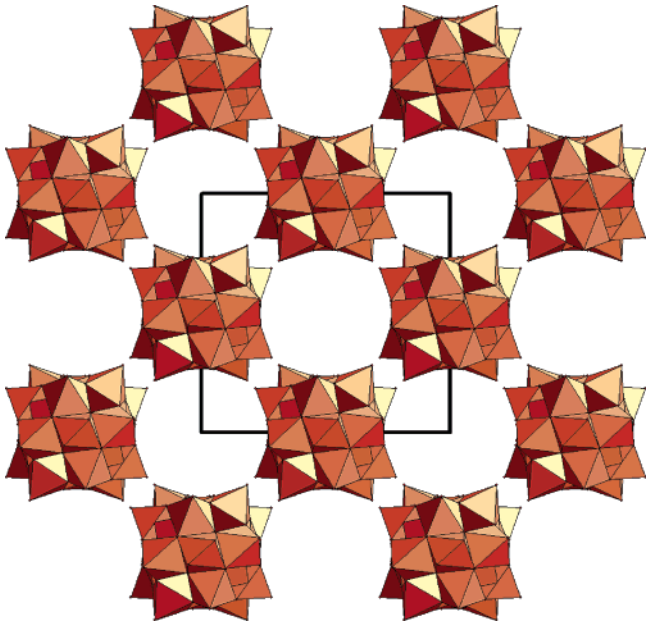

Figure 5. Polyhedral representation of the chains in **K−Nb$_{12}$**, viewed along the *c* axis. (Cations and water molecules omitted.)

the other hand, the radii of the bridging species Ti^{4+} and Nb^{5+} are similar (R_{Ti} = 0.75 Å, R_{Nb} = 0.78 Å),[37] but the difference between the *c* axes of corresponding pairs of phases is larger, about 0.07 Å. The experimentally observed increase in the *c* axis can be expressed as $\Delta c = 0.26\Delta R_{\text{tetrahedral}} + 2.28\Delta R_{\text{bridge}}$, (bridge = Ti or Nb), which compares well with the value $\Delta c = 2\sqrt{2}\Delta R_{\text{bridge}}$ one obtains approximating the bridging species as a pair of regular, edge-sharing octahedra.

Table 7. Cell Parameters of the Four Isostructural Dodecaniobate Keggin Chain Phases[a]

	a (Å)	*c* (Å)	*V* (Å^3)
Nb−Si−Ti	14.2701(5)	11.2923(7)	2299.5(2)
Nb−Si−Nb	14.2649(4)	11.3575(5)	2311.1(1)
Nb−Ge−Ti	14.2852(5)	11.3222(7)	2310.5(2)
Nb−Ge−Nb	14.2633(3)	11.3947(3)	2318.2(1)

[a] Measurement conditions: Angular range, 5−90°; step, 0.04°; 25 s/step. Zero-background quartz plate. Internal standard: NIST Si SRM640, *a* = 5.430898 Å.

(3) Solid-State MAS NMR Spectroscopy. The absence of protons in the structure of **Nb−Si−Ti** was confirmed by ^{1}H solid-state MAS NMR spectroscopy on the as-synthesized sample as well as on a D_2O-exchanged sample. We quantitatively exchanged H_2O for D_2O by stirring the sample in heavy water at room temperature for 2 h to eliminate the potential masking of a small OH signal by the larger signal from H_2O. If the Keggin clusters were protonated, we would have expected a ^{1}H chemical shift around 1.9 ppm, where we observed a peak for monoprotonated sodium hexaniobate.[24] Moreover, weight loss in a temperature range usually corresponding to the elimination of a hydroxyl group (400−600 °C) was not observed by TGA. The NMR results showed that about 90% of H_2O was replaced for D_2O, which, allowing for a partial reexchange with the atmospheric water, indicates that essentially all of the H_2O had been exchanged. ^{29}Si MAS NMR spectroscopy of **Nb−Si−Ti** gives a single peak at −74.4 ppm with a fwhm of 64 Hz, in accordance

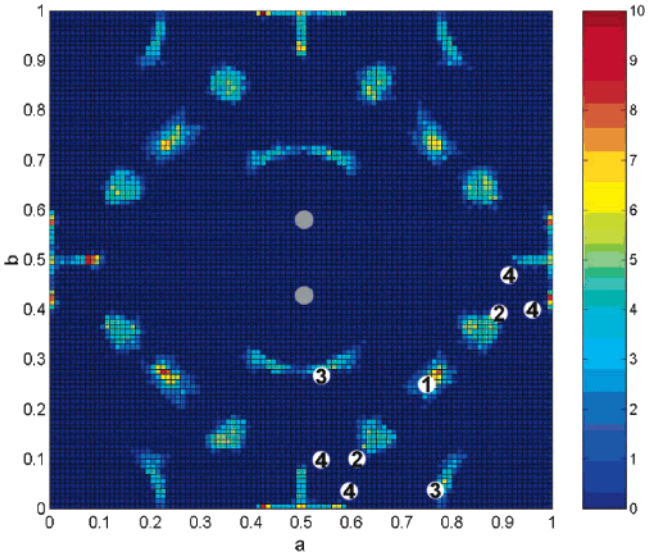

Figure 6. Projection of the probability distribution for sodium cations along the *c* axis of **Nb**−**Si**−**Ti** at 300 K, with an intensity of 10 (highest color intensity) indicating the cubelet with greatest probability of being occupied. Numbered circles: positions of the sites from Rietveld refinement. Sodium cations in site 3 always align themselves with the locally populated O8 oxygen sites (grey circles) of the dimeric bridge.

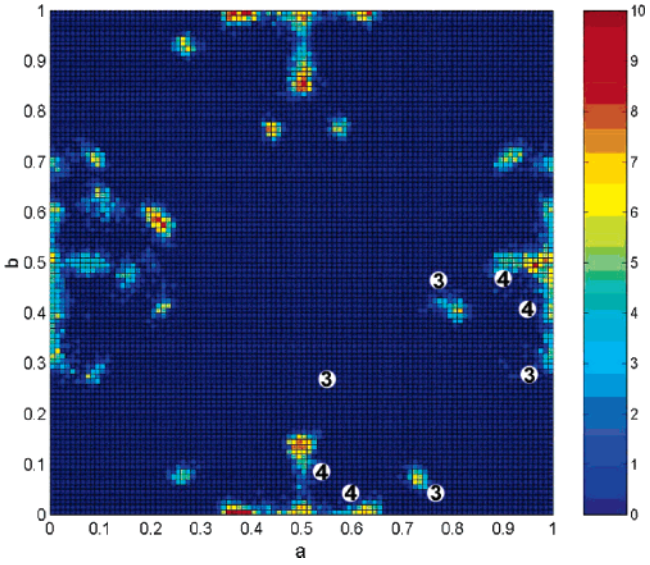

Figure 7. Projection of the probability distribution of water along the *c* axis of **Nb**−**Si**−**Ti** at 300 K.

with the single independent Si site in the structural model. The shift of the resonance closely matches that observed in **K**−**Nb$_{12}$** (−75.9 ppm, fwhm = 80 Hz) where the single Si has a similar environment. Although several Na sites are present in the structure, the ^{23}Na MAS NMR spectrum shows only one broad highly asymmetric resonance centered at −13.2 ppm with a fwhm of 2220 Hz. However, the similarity in the coordination environments of the various sodium sites and the high mobility of the Na^+ ions make differentiation difficult to achieve under usual magnetic field strengths.[38]

(4) Locations of Na^+/H_2O Determined by Molecular Modeling. Figure 6 shows a probability distribution plot for Na^+ in **Nb**−**Si**−**Ti** at 300 K. The distribution plots were computed by discretizing the unit cell into cubelets and recording the fraction of time a given cubelet was occupied by the center of mass of a Na^+ ion or H_2O molecule. The most probable location was assigned an intensity of 10 (highest color intensity), with other location intensities scaled to this value. It is apparent that Na^+ localizes near the four experimentally determined sites (sites 1−4). This indicates that the model is able to locate these positions accurately and does not give spurious sites for Na^+. Sites 1 and 2 were found to be essentially fully occupied by sodium. Practically no water was observed near site 1. The simulations indicate that site 2 sodium atoms coordinate with four framework oxygen atoms at less than ∼3.1 Å. In addition, the sodium cations in site 2 gain additional stability from neighboring water molecules to give a total coordination number close to six at a distance of roughly 3.3 Å. Two-thirds of the sodium atoms required for charge balancing are located at these two well-defined sites. Sites 3 and 4 were found to be only partially occupied by sodium. The sodium cations in these sites were more mobile than those in sites 1 and 2. The simulations indicate that sodium associated with site 3 can rapidly migrate back and forth near the experimental position, as can be seen by the rather broad crescent-shaped occupancy region in Figure 6. The experimental site 3 position is located near the $[Ti_2O_2]^{4+}$ bridges that link the Keggin clusters together along the *c* axis. Within these bridges, the oxygen atoms are disordered, with O8 having an occupancy of 50%. Figure 6 illustrates that Na^+ ions associated with site 3 will occupy only the sites that align with the O8 oxygen atoms, thereby increasing their total coordination number. As expected, the water is significantly more mobile than the sodium cations, exploring much of the region between sites 2, 3, and 4 (observed in Figure 7). Given its high mobility, only ∼30% of the water could be classified into experimental sites, where it primarily occupies sites 3 and 4. The remaining water molecules migrate among sites 2−4, where they hydrate the neighboring sodium cations. The average fractional coordinates and population fractions are reported in Table 4.

With the replacement of Ti^{4+} by Nb^{5+} in the bridging unit for **Nb**−**Si**−**Nb**, the amount of counterbalancing sodium cations needed for charge neutrality decreases, accompanied perhaps by an increase in the amount of water in order to fill the vacant sodium sites. The simulations indicate that, as with structure **Nb**−**Si**−**Ti**, sites 1 and 2 are essentially fully occupied by sodium, containing 80% of the required charge-balancing sodium. The remaining 20% are located in site 4. Unlike structure **Nb**−**Si**−**Ti**, however, the presence of sodium cations in site 3 of **Nb**−**Si**−**Nb** is negligible, as can be seen by comparing Figure 6 with Figure 8, which shows the distribution of Na^+ at 300 K. The population fraction for Na^+ is only 4% for site 3 (see Table 5), indicating that the addition of Nb has made this site less favorable. The depopulation of sodium from site 3 can perhaps be explained by examining its neighboring environment. Site 3 is located near the bridging $[Ti_2O_2]^{4+}$ or $[Nb_2O_2]^{6+}$ units.

(38) Cherry, B. R.; Nyman, M.; Alam, T. M. *J. Solid State Chem.* **2004**, *177*, 2079.

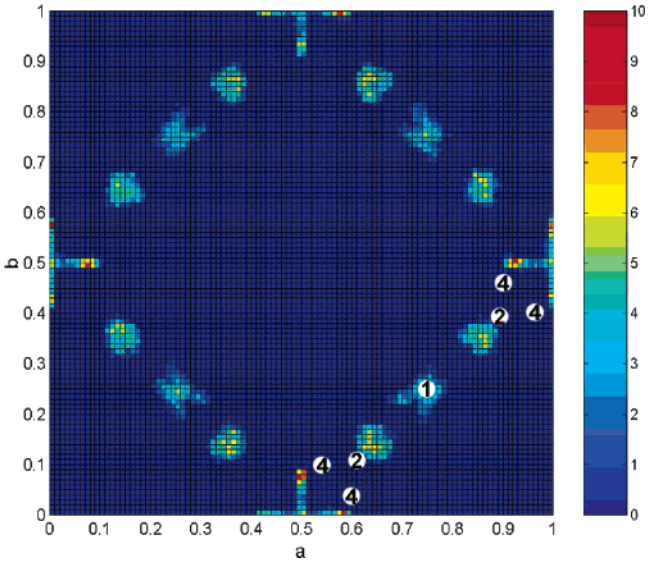

Figure 8. Projection of the probability distribution of sodium cations along the *c* axis of **Nb−Si−Nb** at 300 K. The presence of Nb^{5+} in the Keggin bridging units causes Na^+ to depopulate site 3 relative to structure **Nb−Si−Ti**.

When Nb^{5+} is substituted for Ti^{4+}, the positive charge on the bridging units increases, resulting in greater electrostatic repulsion between the bridge and the surrounding sodium cations. This prevents the Na^+ ions from coordinating with the O8 bridging oxygen atoms, thereby destabilizing the sodium cations located in site 3. Site 4 is situated far enough from the bridging units to be unaffected by this substitution of Nb for Ti. The sodium population on site 4 even increases slightly to compensate for the depopulation of site 3 and still maintain charge neutrality. Coordination numbers for sodium in sites 1, 2, and 4 of **Nb−Si−Nb** are similar to those of **Nb−Si−Ti**.

As with structure **Nb−Si−Ti**, water is observed to reside in a relatively diffuse region near sites 2−4 of structure **Nb−Si−Nb**. In addition, the population fraction for water in site 4 increases because of the expected increase of the water loading in the **Nb−Si−Nb** structure as compared to that in the **Nb−Si−Ti** structure. The simulated sodium and water fractional atomic coordinates and population fractions for **Nb−Si−Nb** are given in Table 5.

(5) Interaction of Sodium with the Keggin Chains. Although the chains in **Nb−Si−Ti** are not strongly bonded to each other *per se*, they are nevertheless connected via their interaction with the sodium atoms. The bridging oxygen atoms of the apical "4-ring windows" of one cluster (O3 and O4) are bonded to a Ti atom (or a Nb atom in the case of **Nb−Si−Nb**) that forms the dimeric bridge linking the Keggin ions together along the *c* axis. The four remaining equatorial windows, comprising the bridging oxygen (O_b) O5 and O6, host a sodium atom (located on site 1) that is also bonded to two terminal oxygen atoms (O_t) O2 of two different clusters of an adjacent chain (see Figure 9a and 9b). This mode of linking three separate Keggin ions via a counterion bonded to four bridging and two terminal oxygen atoms is similarly encountered in $Na_{16}[SiNb_{12}O_{40}]\cdot 4H_2O$:[21] every 4-ring window of the two independent $[SiNb_{12}O_{40}]^{16-}$ ions present in this phase does indeed host a sodium atom, which shows the attractiveness of such a site. Likewise, in **K−Nb$_{12}$**, these equatorial windows host a potassium atom that is in turn, however, only bonded to water molecules and hence does not link directly the neighboring chains together. The sodium atom situated on site 2 in **Nb−Si−Ti** links two clusters from different chains together, by binding an O_t and an O_b of each cluster (see Figure 9a and 9b). This Na atom is also coordinated by the water molecules mostly located around site 4.

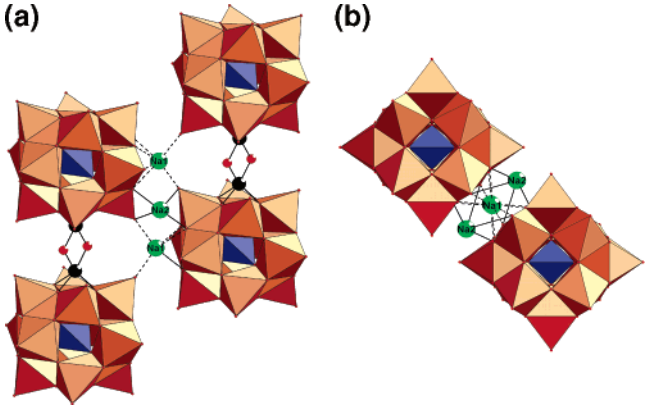

Figure 9. Environment of the sodium atoms present on sites 1 and 2, viewed (a) along the *ab* plane and (b) along the *c* axis. (Water molecules omitted.)

Water Content Determination. Although the exact number of cations in these phases is constrained by charge neutrality, it is possible that the actual amount of water present varies from the compositions derived from the crystal structure refinement (i.e., four H_2O molecules per Keggin cluster for **Nb−Si−Ti** and six H_2O molecules per Keggin cluster for **Nb−Si−Nb**), owing to the difficulty in determining exact loadings of the highly mobile water from X-ray powder diffraction data. The amount of water determined by TGA on the purest samples available synthesized by the hexaniobate route was indeed always found to be much higher than that expected from the structural refinement: 10.6 wt % as found by TGA versus 3.2 wt % calculated for **Nb−Si−Ti** assuming four water molecules per Keggin cluster. Although the presence of highly hydrated amorphous impurities (such as hydrated sodium titanates[39]) could partially explain this discrepancy, this was deemed unlikely on the basis of the SEM examination of the samples, which did not reveal a sizable amount of impurities. Elemental analyses by ICP-MS agree well with the expected composition taking into account this higher water content, which confirms that the amount of impurities is minimal: Na = 10.1 wt %, Ti = 3.7 wt %, and Nb = 42.8 wt % observed; Na = 11.3 wt %, Ti = 3.9 wt %, and Nb = 45.7 wt % calculated. About one-third of the total weight loss observed by thermogravimetry can be obtained by flowing dry nitrogen at room temperature over a sample that was equilibrated with the atmosphere at about 30% relative humidity. We do not think that this initial weight loss is due to the desorption of surface

(39) Anthony, R. G.; Phillip, C. V.; Dosch, R. G. *Waste Manage.* **1993**, *13*, 503.

water because the sample consists of small but well-faceted crystals (see the SEM image in the Supporting Information) and hence should have a low surface area. Rather, we attribute this behavior to the loosely bound interstitial lattice water. Under a heating rate of 10 °C/min, we observe two endothermic events, peaking at 75 and 200 °C, that correspond to about 5 wt % loss each. The second event is most likely the loss of the more tightly bound crystallization water. Furthermore, the facile total D_2O/H_2O exchange and the molecular dynamics simulations had indicated that the water molecules are extremely labile and mobile in this family of compounds. Because of their high atomic displacement parameters, the contribution of the water molecules to the diffracted intensities might be smaller than expected, which would make their detection difficult, especially by Rietveld refinement. Monte Carlo (MC) simulations were used to verify that the structure could indeed accommodate the amount of water found by TGA (14.5 water molecules per Keggin cluster, or 29 water molecules per unit cell) and to study the influence of these extra water molecules on the siting of the sodium atoms.

The water molecules were first removed from a $Na_{12}[Ti_2O_2][SiNb_{12}O_{40}]\cdot 4H_2O$ MD snapshot at 300 K, while leaving the sodium cations in their equilibrated positions. The previous MD simulations showed sodium to be well localized at 300 K, which leads to the assumption that these positions will be essentially the same in the highly hydrated **Nb−Si−Ti·14.5H$_2$O** structure. Two hundred thirty-two water molecules (29 per unit cell) were then randomly inserted into a $2 \times 2 \times 2$ supercell while sodium cations were held fixed at the equilibrated positions determined through MD. When inserting the water molecules, we used antibumping constraints preventing any contact closer than 1.8 Å in order to start with a sensible initial configuration. Monte Carlo (MC) simulations in the canonical ensemble were then performed on the fully hydrated structure for 5 million steps at 3000 K and then quenched for 20 million steps at 300 K to allow the system to equilibrate. As was done previously in the MD simulations, the Keggin chains were kept fixed throughout this process while the sodium atoms and the water molecules were allowed to move without any symmetry or antibumping constraints. In these MC simulations, the more traditional SPC water model[40] was used rather than the fully flexible water model used in the previous MD calculations. The rigid SPC model requires far less computational effort than the flexible water model, which becomes a critical issue as the number of water molecules in the system increases. Furthermore, we have found that the water loading and conformation in zeolites and related open-framework materials are relatively insensitive to the choice of water model. Thus, it is appropriate to test the feasibility of loading the system with 29 water molecules per unit cell with any reasonable model of water. We note that, in using the SPC water model, the Kiselev convention[41] is also employed, where the short-range van der Waals interatomic interactions between the water molecule oxygen atoms and the silicon, titanium, and niobium atoms are neglected because of shielding effects by the framework oxygen atoms. Table 6 shows the averaged Na^+/H_2O positions for sites 1−4 in the **Nb−Si−Ti·14.5H$_2$O** structure. The agreement with experiment is superior to that obtained from the MD simulations of **Nb−Si−Ti·4H$_2$O**, which indicates that this highly hydrated structure might indeed be a better representation of the actual compound than the models with low water content. Figure 10 shows sites 1−3 coordinating with one to two additional water molecules as compared to **Nb−Si−Ti·4H$_2$O**, while site 4 coordinates with three additional water molecules at 3.0 Å. Site 4 is located in a rather large void space between Keggin clusters, thereby enabling it to accommodate more water than the other three sites. The coordination number plots show essentially no sodium−oxygen distances below 2.0 Å. The calculated radial distribution functions in the equilibrated structure for water−water and water−framework interactions show that the closest distances are found between oxygen(SPC)−hydrogen and oxygen(framework)−hydrogen at approximately 1.7 Å, which corresponds to hydrogen-bonding distances.[42] This behavior is consistent with the previous MD results, thereby indicating that the separation distances are reasonable, even at such a high water loading. These MC simulations results indicate that the amount of water found by thermogravimetry can indeed fit between the Keggin chains without requiring unphysical conformations. The void volume calculated using the van der Waals radii of the framework atoms amounts to about only 20 Å^3 per sodium ion or water molecule present in the phase, but this gives only a very crude and, in this case, misleading approximation because it considers the sodium cations, water molecules, and framework atoms as hard spheres of fixed volumes. Figure 11 shows the H_2O probability distribution plot along the *c* axis of the **Nb−Si−Ti·14.5H$_2$O** structure, which shows water locating near sites 2−4. No water was found in site 1, ∼9% of the total water amount was found in site 2, ∼42% was found in site 3, and ∼31% was found in site 4. The remaining ∼18% of water was not associated with one of the sites within the specified 2.0-Å cutoff.

Figure 12 shows the powder diffraction patterns calculated from a single snapshot close to equilibrium for the **Nb−Si−Ti·4H$_2$O** MD model and **Nb−Si−Ti·14.5H$_2$O** MC model. The main difference lies in the overall relative intensities of the low-angle peaks with respect to the rest of the pattern, the influence of the water molecules becoming negligible above ∼30° because of their high atomic displacement parameters. The effects of experimental factors such as the surface roughness of the specimen, the transparency in a non-infinitely thick sample, and the aperture of the divergence slit are difficult to model accurately and will mostly affect the intensities of the low-angle diffraction peaks, which are most sensitive to the water content in these phases. The population parameters refined by the Rietveld

(40) Berendsen, H. J. C.; Postma, J. P. M.; van Gunsteren, W. F.; Hermans, J. In *Intermolecular Forces*; Pullman, B., Ed.; Reidel: Dordecht, The Netherlands, 1981.

(41) Kiselev, A. V.; Lopatkin, A. A.; Schulga, A. A. *Zeolites* **1985**, *5*, 261.

(42) Boulougouris, G. C.; Economou, I. G.; Theodorou, D. N. *J. Phys. Chem. B* **1998**, *102*, 1029.

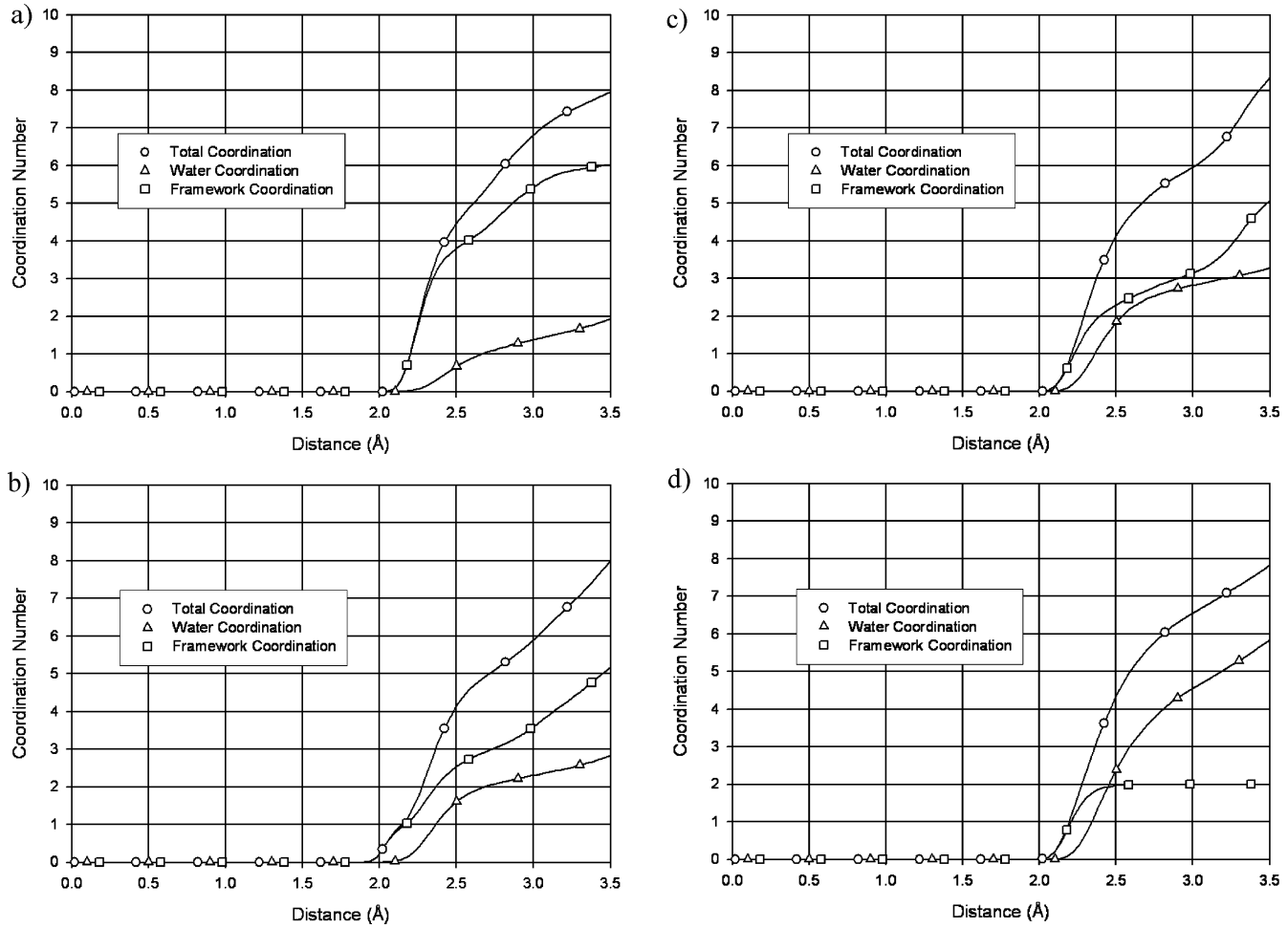

Figure 10. Simulated coordination number of sodium cations in (a) site 1, (b) site 2, (c) site 3, and (d) site 4 in **Nb−Si−Ti·14.5H$_2$O**.

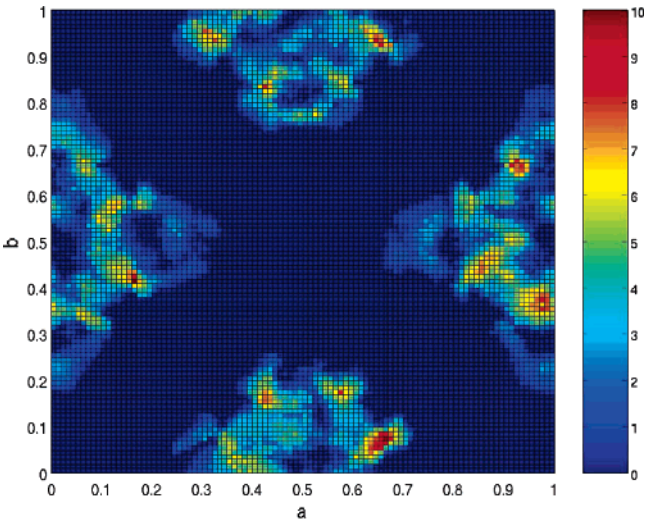

Figure 11. Projection of the probability distribution of water along the *c* axis of **Nb−Si−Ti·14.5H$_2$O** at 300 K. Water is located near sites 2−4.

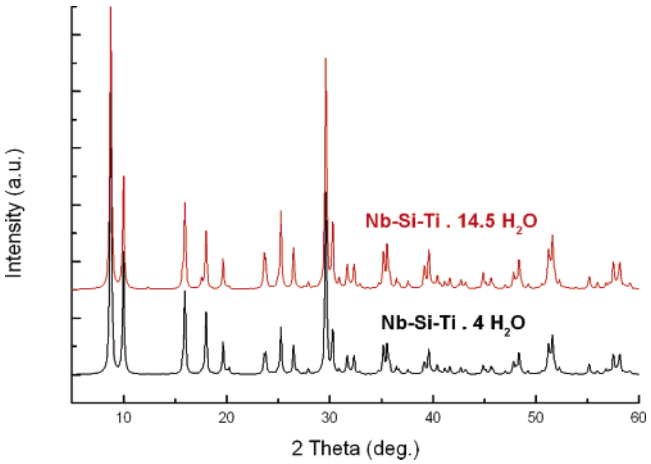

Figure 12. Calculated powder diffraction patterns for the **Nb−Si−Ti·4H$_2$O** MD model and the **Nb−Si−Ti·14.5H$_2$O** MC model.

method are always highly correlated with both the atomic displacement parameters and the background and thus can be very unreliable, especially for light and mobile species. The MC calculations coupled with reproducible TGA results give reason to believe that there might be much more water in these systems than could be located from powder X-ray diffraction data.

Conclusions

In this study, we have synthesized and characterized a series of four isostructural dodecaniobate Keggin chain compounds that have the general formula $Na_{12}[Ti_2O_2][TNb_{12}O_{40}]\cdot xH_2O$ or $Na_{10}[Nb_2O_2][TNb_{12}O_{40}]\cdot xH_2O$ where T = Si or Ge. They were synthesized hydrothermally using the Lindqvist-ion salt $Na_7H_3O[Nb_6O_{19}]\cdot 14H_2O$ as the soluble precursor for both sodium and niobium. These phases could

be obtained only as microcrystalline powders, and their structure was determined ab initio from X-ray powder diffraction data. The inherently lower quality of powder diffraction data compared to single-crystal data made the characterization of the charge-balancing sodium cations and the highly mobile water molecules contained in the interchain regions difficult. Molecular dynamics simulations provided insight into these issues, initially confirming the sodium and water positions determined from the structure refinement. However, thermogravimetry suggested there were approximately 14.5 water molecules per formula unit, rather than the 4−6 water molecules that could be located by the crystal structure analysis. Monte Carlo simulations showed that this higher amount of water could in fact be accommodated by the structure without leading to unreasonable bond distances. This combined approach using crystallography, physicochemical characterizations, and computational studies provided the most accurate model of these materials, especially of the location and quantification the interchain molecular water. Characterization of molecular water in solid-state materials can be challenging, yet it is extremely important for a full understanding of the relationship between material structure and material properties, such as ion-exchange capacity.

Ongoing studies on these dodecaniobate Keggin chain materials are focused on their performance as rapid, high-capacity ion-exchange materials, characteristics resulting directly from the high negative charge of the Keggin chains and the mobility of the interchain species. These studies will include experimental characterization and molecular modeling of ion-exchanged forms of these materials, *in situ* X-ray diffraction studies of the ion-exchange process, and measurements of selectivity for key radionuclides in the Savannah River Site nuclear wastes.

Acknowledgment. This research was supported by Sandia's Laboratory Directed Research and Development program and the U.S. Department of Energy, Office of Science Environmental Management Science Program, Grant DE-FG07-1ER63282. Sandia is a multiprogram laboratory operated by Sandia Corporation, a Lockheed Martin Company, for the U.S. Department of Energy's National Nuclear Security Administration under Contract DE-AC04-94AL85000.

Supporting Information Available: Two X-ray crystallographic files in CIF format, atom labeling scheme in Nb−Ti−Si, IR spectra of Nb−Si−Ti and related phases, TGA-DTA diagram of Nb−Si−Ti, simulated coordination number of sodium in Nb−Si−Ti and SEM of Nb−Si−Ti. This material is available free of charge via the Internet at http://pubs.acs.org.

IC048847+